

**Special Section:**

Exploration of the Activity of Asteroid (101955) Bennu

**Key Points:**

- Meteoroids derived from comets strike Bennu near perihelion once every 2 weeks on average with an impact kinetic energy  $>7,000$  J
- They can explain the particle sizes ( $<10$  cm), speeds ( $<3.3$  m s<sup>-1</sup>), and timing (late afternoon) of Bennu's largest observed particle ejection events
- For meteoroid impacts to match observations, Bennu's surface must be as porous and structurally weak as common soils

**Correspondence to:**W. F. Bottke,  
bottke@boulder.swri.edu**Citation:**

Bottke, W. F., Moorhead, A. V., Connolly, H. C., Jr, Hergenrother, C. W., Molaro, J. L., Michel, P., et al. (2020). Meteoroid impacts as a source of Bennu's particle ejection events. *Journal of Geophysical Research: Planets*, 125, e2019JE006282. <https://doi.org/10.1029/2019JE006282>

Received 19 NOV 2019












Accepted 23 APR 2020

Accepted article online 18 MAY 2020

©2020. The Authors.

This is an open access article under the terms of the Creative Commons Attribution-NonCommercial-NoDerivs License, which permits use and distribution in any medium, provided the original work is properly cited, the use is non-commercial and no modifications or adaptations are made.

## Meteoroid Impacts as a Source of Bennu's Particle Ejection Events

W. F. Bottke<sup>1</sup> , A. V. Moorhead<sup>2</sup> , H. C. Connolly Jr<sup>3,4</sup> , C. W. Hergenrother<sup>4</sup> , J. L. Molaro<sup>5</sup> , P. Michel<sup>6</sup> , M. C. Nolan<sup>4</sup> , S. R. Schwartz<sup>4</sup> , D. Vokrouhlický<sup>7</sup> , K. J. Walsh<sup>1</sup> , and D. S. Lauretta<sup>4</sup> 

<sup>1</sup>Southwest Research Institute, Boulder, CO, USA, <sup>2</sup>NASA Meteoroid Environment Office, Marshall Space Flight Center EV44, Huntsville, AL, USA, <sup>3</sup>Department of Geology, Rowan University, Glassboro, NJ, USA, <sup>4</sup>Lunar and Planetary Laboratory, University of Arizona, Tucson, AZ, USA, <sup>5</sup>Planetary Science Institute, Tucson, AZ, USA, <sup>6</sup>Université Côte d'Azur, Observatoire de la Côte d'Azur, CNRS, Laboratoire Lagrange, Nice, France, <sup>7</sup>Institute of Astronomy, Charles University, Prague, Czech Republic

**Abstract** Asteroid (101955) Bennu, a near-Earth object with a primitive carbonaceous chondrite-like composition, was observed by the Origins, Spectral Interpretation, Resource Identification, and Security-Regolith Explorer (OSIRIS-REx) spacecraft to undergo multiple particle ejection events near perihelion between December 2018 and February 2019. The three largest events observed during this period, which all occurred 3.5 to 6 hr after local noon, placed numerous particles  $<10$  cm on temporary orbits around Bennu. Here we examine whether these events could have been produced by sporadic meteoroid impacts using the National Aeronautics and Space Administration's (NASA) Meteoroid Engineering Model 3.0. Most projectiles that impact Bennu come from nearly isotropic or Jupiter-family comets and have evolved toward the Sun by Poynting-Robertson drag. We find that 7,000-J impacts on Bennu occur with a biweekly cadence near perihelion, with a preference to strike in the late afternoon ( $\sim 6$  pm local time). This timing matches observations. Crater scaling laws also indicate that these impact energies can reproduce the sizes and masses of the largest observed particles, provided the surface has the cohesive properties of weak, porous materials. Bennu's ejection events could be caused by the same kinds of meteoroid impacts that created the Moon's asymmetric debris cloud observed by the Lunar Atmosphere and Dust Environment Explorer (LADEE). Our findings also suggest that fewer ejection events should take place as Bennu moves further away from the Sun, a result that can be tested with future observations.

**Plain Language Summary** The asteroid Bennu, the target of the OSIRIS-REx sample return mission, was observed to be ejecting tiny rocks shortly after the spacecraft entered orbit. The three largest ejection events took place in the late afternoon local time, with an average interval of 2 weeks. Each event launched multicentimeter-sized and smaller rocks into temporary orbits, where some escaped and others reimpacted Bennu. Given that all inner solar system objects are bombarded by cometary dust particles, we used a NASA model constructed to evaluate spacecraft impact risk to explore whether impacts could be the source of these events. We found that millimeter-sized cometary dust particles not only strike Bennu in the late afternoon, matching observations, but also produce enough ejected debris to explain the orbiting particles, provided that the material being pummeled is weak.

### 1. Introduction

Asteroid (101955) Bennu is the target of National Aeronautics and Space Administration's (NASA) sample return mission Origins, Spectral Interpretation, Resource Identification, and Security-Regolith Explorer (OSIRIS-REx) (Lauretta et al., 2017). Bennu was chosen for two main reasons: It is a small (490-m diameter) asteroid with a spectral signature consistent with primitive, organic-rich carbonaceous chondrite meteorites determined from ground-based astronomical studies (e.g., Lauretta et al., 2015) and confirmed from spacecraft remote sensing data (Hamilton et al., 2019; Lauretta, DellaGiustina, et al., 2019). In addition, it is easily accessible in its Earth-like orbit; Bennu's orbit has semimajor axis, eccentricity, and inclination ( $a$ ,  $e$ ,  $i$ ) values of (1.126 au, 0.204, 6.035°). An unexpected attribute of Bennu is that it is ejecting small particles into space in distinct events.

Multiple particle ejection events were observed between the end of December 2018, the time when OSIRIS-REx entered into Bennu orbit, and February 2019 (Lauretta, Hergenrother, et al., 2019). Bennu reached perihelion in early January, so there may be an association between these events and Bennu's orbital location at that time. Although many smaller events took place throughout this time period, the three largest observed events, in terms of the number of particles ejected, occurred on 6 January, 19 January, and 11 February, corresponding to a roughly biweekly cadence. We will focus on these events in this paper, with key details summarized below from Lauretta, Hergenrother, et al. (2019).

There are several mechanisms that could lead to particle ejection events on Bennu—e.g., volatile escape, thermal fracturing of boulders (Molaro et al., 2020; Rozitis et al., 2020), and/or electrostatic levitation of surface material (Lauretta, Hergenrother, et al., 2019). Here we investigate the possibility that the events could be caused by meteoroid impacts. Small meteoroids, mostly derived from comets, collide with Earth, the Moon, and presumably Bennu at very high speeds. We hypothesize that some of these events are substantial enough to eject material off of Bennu and into trajectories where it can be observed by OSIRIS-REx. To test this scenario, we simulated the primary meteoroid flux onto Bennu using Version 3 of NASA's Meteoroid Engineering Model (MEM 3; Moorhead et al., 2020).

## 2. Constraints on Bennu's Largest Particle Ejection Events

The three events that we study here produced many tens to hundreds of observed particles, all of which were less than  $\sim 10$  cm in diameter and had ejection velocities  $< 3.3$  m s<sup>-1</sup> (Lauretta, Hergenrother, et al., 2019). These sizes should probably be considered upper bounds; new calculations indicate the largest particle was only about 6 cm, with just a small number of particles between 2 and 4 cm (S. Chesley, personal communication). The kinetic energies of the observed particles, as derived from their inferred masses and velocities, were collectively (for each event)  $< 300$  mJ. This limit, however, has potentially been affected by observational selection effects. Fast-moving particles that readily escape Bennu's gravitational pull quickly fall below the detection limit of OSIRIS-REx. Accordingly, it is plausible that we have only observed the low-velocity tails of larger ejecta fragment distributions.

Dynamical simulations of the observed particles indicate that they emanated from several regions across Bennu. Each set of particles seems to have been ejected at the same time, though existing data are not precise enough to rule out the possibility that a short interval lasting seconds to minutes took place between the ejection of the first and last particles. Follow-up observations of the ejection sites do not yet show any unusual characteristics, though existing images are not yet capable of seeing details smaller than a few meters. There have been no detections of released volatiles, a coma, or any recent large-scale mass movement on Bennu that might launch debris into orbit.

All three events took place in the late afternoon, between 15:22 and 18:05 local Bennu time (i.e., about 3.4 to 6 hr after local noon). They also took place within days to weeks of Bennu reaching perihelion, though given the relatively low eccentricity of Bennu and limited observations, it is not yet clear whether this is an influential factor for the putative ejection event mechanism. The albedo distribution of the particles is difficult to determine with precision from the existing data. If the particles are assigned bulk densities of  $\sim 2$  g cm<sup>-3</sup>, a value that matches the bulk densities of CM and CI meteorite data (Scheeres et al., 2015), the albedos would range from 0.05 to 0.3. For reference, the net surface area of rocks on Bennu with albedos  $> 7\%$  is  $< 1\%$  (Lauretta, DellaGiustina, et al., 2019). Alternatively, if we assume the particles had albedos of  $\sim 4\%$ , the same as Bennu's global geometric albedo (4.4%; Lauretta, DellaGiustina, et al., 2019), the particle densities would be lower than 2 g cm<sup>-3</sup>.

## 3. MEM

MEM 3 describes the mass-limited flux, directionality, velocity, and density distribution of meteoroids impacting a target body orbiting between Mercury and the asteroid belt (e.g., McNamara et al., 2005; Moorhead et al., 2020). A common application of MEM is to evaluate impact risk and potential damage to Earth-orbiting satellites (e.g., the International Space Station) and spacecraft traveling in the inner solar system. MEM builds on several studies of the interplanetary dust population and the nature of the near-Earth environment, some of which will be briefly described below.

MEM specifically models the sporadic component of the meteoroid environment, that is, those meteoroids not affiliated with a meteor shower. For particles <0.5 cm, less than 10% of the net fraction of impactors hitting Earth are from showers (Moorhead et al., 2017). Thus, showers are considered by the authors of MEM to be a minor contributor to spacecraft risk and are not included.

As an additional check on the importance of showers for Bennu impacts, we examined the International Astronomical Union database of meteor streams, specifically those from Jenniskens et al. (2016), and calculated the minimum distance between them and Bennu's orbit. We found a few streams that may be close enough to Bennu to represent an increase in the impact flux (i.e.,  $\eta$  Virginids,  $\kappa$  Serpentids were within 0.01 au), but they are also rather weak. We also looked for meteor showers that cross the ecliptic plane within  $10^\circ$  of Bennu's perihelion (longitude of  $\sim 68^\circ$ ), which is a typical-to-generous shower duration. As before, we found a few candidate showers ( $\sigma$  Hydrids,  $\varepsilon$  Aquilids,  $\alpha$  Monocerotids, November Orionids, Southern  $\chi$  Orionids), but they were also weak sources. For these reasons, we do not consider streams further in this analysis.

The meteoroid directionality and velocity distributions output by MEM are derived from several orbital populations modeled by Jones (2004). Jones assumed that meteoroids originated from four parent body groups: long-period comets, Halley-type comets, Jupiter-family comets, and asteroids. To parameterize their orbital distribution within the model, Jones (2004) assumed that particles from each population are affected by radiation pressure, Poynting-Robertson drag, and collisions. By estimating the signatures of particles from each population near Earth, it becomes possible to fit the parametric model to observational data, with the strength of the particle sources determined by the fit. Here the constraints come from the distribution of sporadic meteor radiants and velocities observed from the Canadian Meteor Orbit Radar network and zodiacal light data from the Helios I and Helios II missions (see also Moorhead et al., 2020).

The sources of sporadic meteoroid activity have been assigned names according to where they have been observed in the sky. Apex particles, north and south, mainly come from long-period comets and are often on retrograde orbits. Many encounter Earth, Moon, and other inner solar system bodies such as Bennu in the "head-on" direction with respect to the object's path around the Sun, much like insects striking a car's windshield. Accordingly, the impact velocities of these particles can be very high, commonly  $\sim 50$  to  $60 \text{ km s}^{-1}$ . The helion and antihelion sources are from Jupiter-family comets. These particles have lower inclinations and encounter Earth from the solar and antisolar directions, respectively, at velocities of tens of kilometers per second. Toroidal meteoroids, north and south, are highly inclined to the ecliptic and come from Halley-type comet particles. They can also hit at high velocities, though less high than the apex and helion/antihelion meteoroids on average in MEM (Jones, 2004). Modeling work indicates that asteroid particles are only a minor contributor to the sporadic meteoroid complex (e.g., Jones, 2004; Nesvorný et al., 2010); MEM 3 excludes them.

The overall magnitude of the meteoroid flux as modeled by MEM is tied to the meteor flux measured by the Canadian Meteor Orbit Radar (Jones, 2004; Jones et al., 2005); the specific anchor point is the flux at the top of Earth's atmosphere (Moorhead et al., 2020). The uncertainty associated with MEM, or indeed any meteoroid model, is not well characterized but is expected to grow with increasing geocentric distance. MEM is therefore restricted to modeling the meteoroid environment in the inner solar system and only accepts trajectories with heliocentric distances between 0.2 and 2 au.

MEM's mass-limited flux is similar, but not identical, to that given by Grün et al. (1985); furthermore, MEM assumes that the shape of the mass distribution can be described using the Grün et al. (1985) relation. This relation was developed by assuming that meteoroids are affected by radiative forces and collisions but are in a steady state. Here  $g(m)$  is the Grün et al. flux of meteoroids at 1 au. It assumes that the number of particles per square meter per year larger than a limiting mass  $m$  in grams is impacting a randomly oriented flat plate under a viewing angle of  $2\pi$ .

$$g(m) = (c_4 m^{\gamma_4} + c_5)^{\gamma_5} + c_6 (m + c_7 m^{\gamma_6} + c_8 m^{\gamma_7})^{\gamma_8} + c_9 (m + c_{10} m^{\gamma_9})^{\gamma_{10}}. \quad (1)$$

The constants are  $c_4 = 2.2 \times 10^3$ ,  $c_5 = 15$ ,  $c_6 = 1.3 \times 10^{-9}$ ,  $c_7 = 10^{11}$ ,  $c_8 = 10^{27}$ ,  $c_9 = 1.3 \times 10^{-16}$ , and  $c_{10} = 10^6$ . The exponents are  $\gamma_4 = 0.306$ ,  $\gamma_5 = -4.38$ ,  $\gamma_6 = 2$ ,  $\gamma_7 = 4$ ,  $\gamma_8 = -0.36$ ,  $\gamma_9 = 2$ , and  $\gamma_{10} = -0.85$ . These constants and exponents require  $m$  to be expressed in grams and yield a flux in units

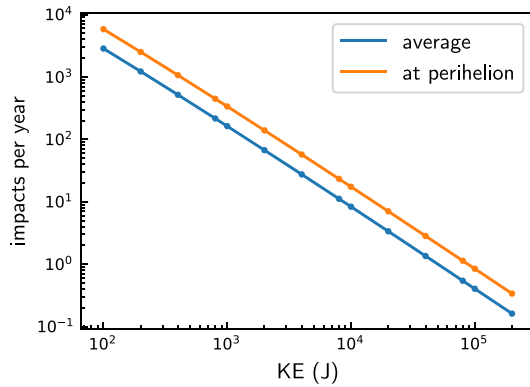


**Figure 1.** The impact rate of meteoroids on Bennu as a function of limiting kinetic energy. We find that collisions with kinetic energies of 4,000 J (4 kJ) take place approximately once every 2 weeks if we average over the entire orbit, the same cadence as the three largest particle ejection events observed to date on Bennu. If we concentrate on impacts at perihelion, where the impact rate is higher, 7,000 J (7 kJ) impacts are delivered biweekly.

of square meter per second. The meteoroid fluxes generated by MEM have the same mass dependence, but not magnitude, as the Grün et al. flux. We can use the Grün equation (Equation 1) to rescale MEM's fluxes to a different mass. Or, in other words, if  $m_0$  is our reference mass and  $f$  is the meteoroid flux computed by MEM for a given mass  $m$ , then  $f(m) = f(m_0)g(m)/g(m_0)$ . Thus, MEM uses the Grün et al. relation to scale the flux to the user's desired limiting mass, and the Grün et al. relation can also be used in postanalysis to scale the results to, for instance, a constant limiting kinetic energy ( $KE$ ).

MEM is limited to describing those particles with masses capable of doing damage to spacecraft, namely, those that are between  $10^{-6}$  and 10 g. Smaller particles are not modeled; their orbits are more strongly modified by radiation pressure and Poynting-Robertson drag and may therefore have a different orbital distribution than the one assumed by MEM.

The meteoroid density distribution in MEM is bimodal, with a low and a high bulk density component. Sporadic meteoroids from nearly isotropic comet sources are assigned to the low bulk density component, with values ranging between 400 and 1,600  $\text{kg m}^{-3}$ . A meteoroid's value is chosen randomly from a normal probability distribution, with the highest

probability being 860  $\text{kg m}^{-3}$  (Moorhead et al., 2020). The helion and antihelion meteoroids are assumed to be in the high bulk density component, with values ranging between 2,500 and 8,000  $\text{kg m}^{-3}$  (Moorhead et al., 2020). The most probable value is 3,800  $\text{kg m}^{-3}$ . Many of these particles are cometary, but it is assumed that their exposure to solar radiation and their more frequent close passages to the Sun increase their density to approximately asteroidal values.

The MEM model has been verified against impacts on the Pegasus II and III satellites and the Long Duration Exposure Facility (Moorhead et al., 2020). MEM results match observations within a factor of 3. For this reason, we find MEM to be useful for exploring the nature of meteoroid impacts on Bennu, a near-Earth object with an Earth-like orbit.

#### 4. Model Runs

An ephemeris for Bennu was obtained from the JPL Horizons On-Line Ephemeris System (<https://ssd.jpl.nasa.gov/horizons.cgi>); we downloaded state vectors for the asteroid at 1-day intervals between 10 January 2019 and 22 March 2020. We thus consider one orbital period of the asteroid, starting with its 2019 perihelion passage. Technically, this period excludes a portion of the period during which particle ejection events were observed, but the orbital elements of Bennu are effectively static for our purposes.

MEM generates a mass-limited flux for a given target; the code also divides the total flux into bins by the angle and speed with which they encounter the target. However, the amount of material generated by a crater-forming impact event is generally held to be a function of the impactor's  $KE$  (e.g., Melosh, 1989). Thus, we use Equation 1 to scale the flux in each bin to the same  $KE$  and sum the results to find the overall  $KE$ -limited flux of meteoroids onto Bennu. In other words, we determine the limiting mass for each velocity in a bin with index  $i$  ( $V_i$ ) that corresponds to our the  $KE$  threshold ( $2 KE/V_i^2$ ), and we then scale the flux to the limiting mass using the Grün relationship in Equation 1 ( $g(m)$ ). This method yields

$$f(KE) = \sum_i f_i(1 \mu\text{g}) g(2 KE/V_i^2) / g(1 \mu\text{g}). \quad (2)$$

where  $f(KE)$  is the total flux of meteoroids with a kinetic energy of  $KE$  or greater, and  $f_i(1 \mu\text{g})$  is the flux of meteoroids of mass 1  $\mu\text{g}$  or greater in velocity bin  $i$ .

This means that for  $V_i = 40 \text{ km s}^{-1}$  versus  $20 \text{ km s}^{-1}$ , our method includes masses four times smaller. Because  $g(m)$  is close to a power law, the correction is further steepened (i.e.,  $\sim 4^{-1.34} = 6.4$ ; see below). Accordingly, much of the flux will come from small but fast-moving particles. This method also explains

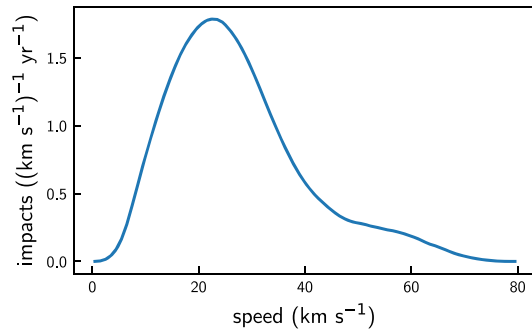


**Figure 2.** Impact velocity distribution of sporadic meteoroids on Bennu that have masses of at least 5 mg. The integral of the area under the curve equals the mass-limited flux. The y-axis is the number of impacts that occur per year at a given impact velocity. The peak velocities are slightly larger than  $20 \text{ km s}^{-1}$ . The high-velocity tail becomes important when we consider the kinetic energy of impactors on Bennu.

This limiting energy is 26,000 times that of the energy estimated for the largest particle ejection event on 6 January (i.e., 270 mJ) (Lauretta, Hergenrother, et al., 2019). If a small fraction of impact energy goes into particle ejection, these results indicate that meteoroid impact events provide more than sufficient energy to reproduce observations. Whether 7-kJ impacts can reproduce the observed ejected particles will be discussed in section 5.1.

The impact velocity distribution for meteoroids striking Bennu is shown in Figure 2 for a limiting mass of at least 5 mg. MEM assumes no mass dependence with velocity. The dominant peaks come from Jupiter-family comet particles (helion and antihelion sources) that have been circularized enough by Poynting-Robertson drag that they can strike Bennu at relatively low velocities. The peak of this distribution is slightly larger than  $20 \text{ km s}^{-1}$ .

When considering the effects of impacts onto Bennu, we need to concern ourselves with the combination of mass ( $m$ ) and impact velocity ( $V$ ). A proxy for their behavior when making small craters on Bennu is  $KE$  ( $KE = 0.5 m V^2$ ). In Figure 1, we showed that at perihelion, Bennu receives a 7-kJ event every 2 weeks. Accordingly, we have created meteoroid impact speeds and masses for this nominal limiting energy of 7 kJ (Figures 3 and 4). Here the highest speeds and lowest masses mainly come from meteoroids derived from the apex source (long-period comet particles on retrograde orbits). The lowest speeds and most massive particles mainly come from Jupiter-family comets (helion and antihelion sources). The average impact speed for 7-kJ impactors is  $42.8 \text{ km s}^{-1}$ .

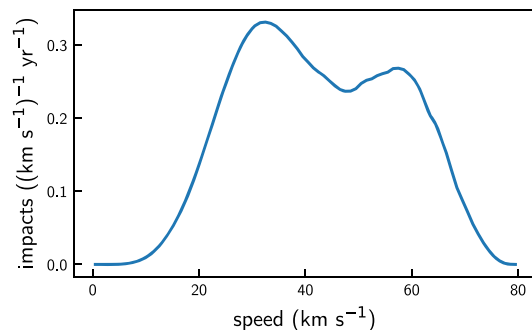


**Figure 3.** Impact velocity distribution of sporadic meteoroids on Bennu that have limiting kinetic energies of 7 kJ. The integral of the area under the curve equals the kinetic energy-limited flux. The y-axis is the number of impacts that occur per year at a given impact velocity. Most of the high velocities come from retrograde meteoroids that originated on long-period comets (apex source). Some also come from high-inclination meteoroids derived from Halley-type comets (toroidal source). Most lower velocities come from meteoroids derived from Jupiter-family comets and asteroids (helion and antihelion sources). The average speed is  $42.8 \text{ km s}^{-1}$ .

why the  $KE$ -limited speed distribution differs from the mass-limited speed distribution, though we will show both. Grün et al. (1985) gave a lower-fidelity description of the meteoroid environment that does not take this issue into account. MEM does not apply the Grün et al. model per se, but a more detailed model that has been validated against observed spacecraft impact rates (Moorhead et al., 2020).

We convert this flux to a cratering rate assuming that Bennu's surface area is  $0.782 \text{ km}^2$  (Lauretta, DellaGiustina, et al., 2019). We show this rate as a function of limiting  $KE$  in Figure 1.

We find that collisions with kinetic energies of 4,000 J (4 kJ) take place approximately once every 2 weeks, the same cadence as the largest particle ejection events observed on Bennu, if we average over Bennu's entire orbit. If we focus our attention to perihelion, where the observed particle ejection events took place, the delivered energy from impacts increases to 7,000 J (7 kJ). This value will be used as our metric in the figures below.

The impact rate on Bennu as a function of mean anomaly at the limiting  $KE$  of 7 kJ is shown in Figure 5. Bennu's perihelion corresponds to a mean anomaly of  $0^\circ$ , whereas aphelion is  $180^\circ$ . The impact rates vary by more than a factor of 5 between perihelion and aphelion. There are several reasons that a higher flux is expected near perihelion. First, the mass-limited number density of meteoroids in MEM is roughly proportional to  $r^{-1.3}$ , where  $r$  is heliocentric distance, following a relation derived from zodiacal light observations (Jones, 2004; Leinert et al., 1981). Second, Bennu tends to encounter meteoroids at higher relative speeds near perihelion (e.g., Bottke et al., 1994). This allows them to sweep up more objects in a given unit of time, which increases the flux. At the same time, the higher speeds lower the mass required to generate an impact of a given  $KE$ ; as a result, the ratio of the  $KE$ -limited flux at perihelion to that near aphelion will be greater still.

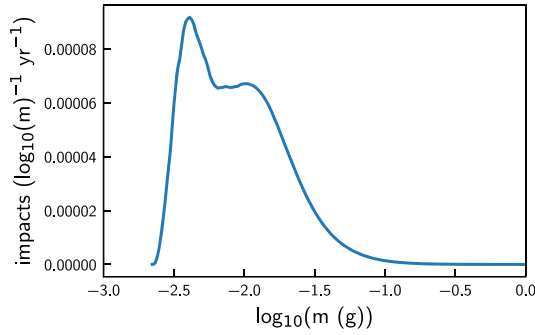


**Figure 4.** Impactor mass distribution ( $m$ ) in grams for meteoroids striking Benu at the limiting kinetic energy of 7 kJ. The y-axis is in units of how many impacts take place at a given mass per year. Note that this is not a distribution of the particle masses incident on Benu but rather the distribution of limiting masses that correspond to our kinetic energy threshold and the velocity distribution (i.e., for each velocity bin, what is the mass that gives us that kinetic energy value). This plot allows us to visually convert our kinetic energy value and speed distribution to equivalent masses; the mass-limited equivalent would be a delta function. The smallest impactors on this plot are hitting at the fastest velocities, with the spike in the smallest mass occurring at  $\sim 60 \text{ km s}^{-1}$  (Figure 2). The mean velocity of  $42.75 \text{ km s}^{-1}$  corresponds to a mass of  $0.00766 \text{ g}$ , whose  $\log_{10}$  value is  $-2.12$ . If we assume the impactor bulk density is  $860$  or  $3,800 \text{ kg m}^{-3}$ , common values used by MEM, this mass corresponds to particles that are  $2.6$  and  $1.6 \text{ mm}$ , respectively.

Benu reached perihelion in early January, close in time to the three largest particle ejection events (6 January, 19 January, and 11 February) observed to date and when impacts should be the most common along Benu's orbit. As Benu moves away from perihelion, MEM predicts that comparable particle ejection events should become rarer. Future observations will be able to test this possibility, though as a caveat, putative particle ejection mechanisms based on peak temperatures and proximity to the Sun may produce a similar pattern.

All plots shown so far give the total number of meteoroid impacts that we expect Benu to experience. The environment, however, is far from isotropic. Instead, the directionality of the meteoroids that encounter Benu are clustered into groups: These are the sporadic sources (i.e., apex and helion sources). Figure 6 displays a directional map of the meteoroid flux. Because Benu's orbit is similar to that of Earth, these sources resemble those observed by meteor surveys (see, e.g., Figure 5 of Campbell-Brown, 2008).

Thus, the number of impacts varies across the surface of Benu; the portion of the surface facing in the direction of Benu's motion, for instance, will sweep up more meteoroids at higher speeds and thus should experience more impacts. A point on the surface of the asteroid is exposed to meteoroids whose radiants lie within  $90^\circ$  of the local normal vector. Thus, the local impact rate is

$$F(\lambda_k, \beta_l) = \sum_{i,j} f(\theta_i, \varphi_j) \cos \alpha_{i,j,k,l} H(\cos \alpha_{i,j,k,l}). \quad (3)$$

$F$  is the computed flux or impact rate through the surface facet,  $\lambda_k$  and  $\beta_l$  are the longitude and latitude of a given point on the surface of the asteroid,  $f$  is the flux perpendicular to a given apparent radiant (i.e., Figure 6),  $\theta_i$  and  $\varphi_j$  describe the direction of a meteoroid impact relative to the asteroid (i.e., its apparent radiant),  $H$  is the Heaviside function, and  $\alpha_{i,j,k,l}$  is the angle between the surface normal vector and the meteor radiant.

We approximate the surface of Benu as a sphere, where the normal vector at any point on its surface is identical to that pointing from the center of the surface to that latitude ( $\beta_l$ ) and longitude ( $\lambda_k$ ):

$$\cos \alpha_{i,j,k,l} = \cos \varphi_j \cos \beta_l \cos(\theta_i - \lambda_k) + \sin \varphi_j \sin \beta_l. \quad (4)$$

In reality, Benu is a top-shaped object (Barnouin et al., 2019), and the mapping between location and normal vector is more complex. We neglect this complexity to obtain a simple overall description of the flux on the surface. The resulting flux over the surface of Benu at perihelion for a limiting  $KE$  of 7 kJ is shown in Figure 7. The coordinate system is defined by the local solar time; the subsolar point is located at the "12 pm" label, and the top and bottom of the plot correspond to ecliptic north and south, respectively. Benu is a retrograde rotator with an obliquity of nearly  $180^\circ$ , and so the vertical dashed line in the middle of the plot corresponds to the evening terminator and is labeled "6 pm".

We find that the majority of impacts should occur in the late afternoon near the terminator. This prediction is an excellent match to the three largest observed particle ejection events that occurred between 15:22 and 18:05 local Benu time. Although more events

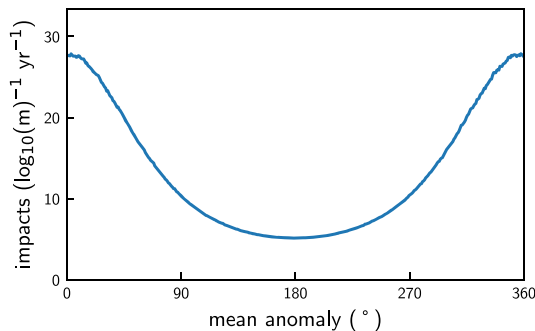


**Figure 5.** The impact rate on Benu as a function of mean anomaly at the limiting kinetic energy of 7 kJ. Benu's perihelion corresponds to mean anomaly of  $0^\circ$ , whereas aphelion corresponds to  $180^\circ$ . The impact rate varies by more than a factor of 5, with most impacts occurring near perihelion. The reason for the change is that Benu is traveling faster near perihelion than near aphelion. This allows Benu to "sweep up" more meteoroids at perihelion (e.g., Bottke et al., 1994) while also increasing the relative speed between Benu and the meteoroids.

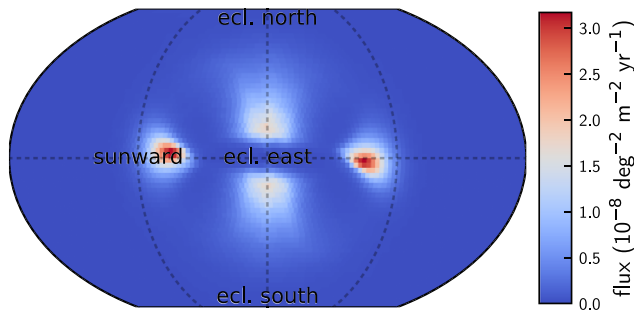


**Figure 6.** The directionality of the meteoroid flux relative to Benu at perihelion for a limiting kinetic energy of 7 kJ. The coordinate system is Sun-centered ecliptic, where the center of the plot points in the direction of increasing ecliptic longitude, or roughly toward Benu's direction of motion. Ecliptic (ecl.) north and south are at the top and bottom of the plot. This is what an observer would see if they were at the center of Benu and scanning the sky for sporadic meteoroids. The apex sources are two concentrations above and below ecliptic east. The helion and antihelion sources are to the left (sunward) and right (antisunward) of ecliptic east, respectively.

and better statistics will be needed to confirm this relationship, impacts are a strong candidate to be Benu's primary particle ejection event mechanism.

Note that Figure 7 is plotted as a *KE*-limited version of these meteoroid impacts. It is possible to also plot a mass limited flux version of the same data set, and it shows signs of the bimodality of the sky sources. When this analysis is performed with the *KE*-limited flux, the high speeds of meteoroids from the “ram” direction are enough to erase the saddle point in the middle of the plot.

We have also calculated MEM's predictions for the directionality of the meteoroid impact flux across the surface of Benu at different locations in its orbit for a limiting *KE* of 7 kJ (Figure 8). As previously noted (see also Figure 4), most impacts should occur near perihelion. As Benu moves away from perihelion, impacts should decrease and shift toward the evening hours. The minimum impact flux should occur near aphelion, while impacts on the inbound orbit should move to the early afternoon.

## 5. Discussion

### 5.1. Impact Ejecta Produced by Meteoroid Impacts on Benu

Our prediction is that a 7-kJ meteoroid impact occurs on Benu once every 2 weeks on average. The next question is whether such collisions can produce the characteristics of the observed particle ejection events discussed above.

Examining Figure 2, we find that the average velocity of these impacts when *KE* is fixed at 7 kJ is  $\sim 43 \text{ km s}^{-1}$ . Using MEM's bulk densities of 860 and 3,800  $\text{kg m}^{-3}$ , and with  $KE = 0.5 m V^2$ , this speed yields into impactor diameters of 2.6 and 1.6 mm, respectively. Our goal is to translate such collision events into an ejecta size-velocity distribution that can be compared with data. One method of doing so is to compare our prospective impacts to crater scaling laws based on laboratory shot experiments.

Accordingly, to test whether the Benu collisions are capable of reproducing the particle ejection event observations, we used the Impact and Explosion Effects web tool written by K. Holsapple and K. Housen (<http://keith.aa.washington.edu/craterdata/scaling/index.htm>; Holsapple, 1980, 1993; Holsapple & Housen, 2013;

Holsapple & Schmidt, 1980, 1982; Housen & Holsapple, 1999, 2011; Housen et al., 1983; Pierazzo et al., 1997; Schmidt & Housen, 1987). This application allows the user to determine the crater size and mass of ejecta formed over a wide range of projectile sizes and target properties. It can be used on water targets and hard rocks where the granular structure of the target material is unimportant. It is based on the so-called Pi-crater scaling methods that have been validated by experiments, field data, and numerical simulations.

#### 5.1.1. Justification of the Use of the Impact and Explosion Effects Web Application

It is possible to question the use of the Impact and Explosion Effects web application for comparing model meteoroid impacts to Benu data. Specifically, the high-velocity impacts discussed in our MEM modeling work have only been tested in a laboratory setting with projectiles that are submicron to micron in size.

For example, Fiege et al. (2019) used a 2-MV Van de Graaff accelerator to examine what happens when micron-sized copper projectiles are propelled into CV and eucrite meteorites. These experiments were designed to examine space weathering on asteroid surfaces. They

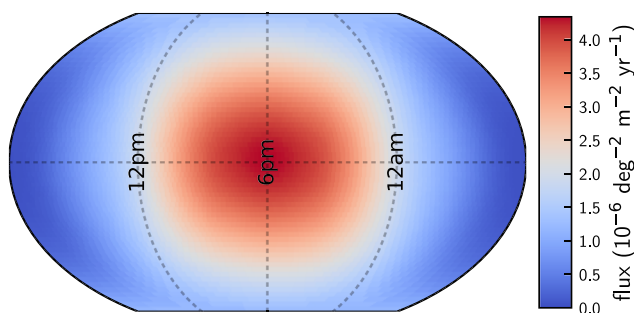


**Figure 7.** The directionality of the meteoroid impact flux across the surface of Benu at perihelion for a limiting kinetic energy of 7 kJ. The coordinate system is Sun-centered ecliptic, and Benu is a retrograde rotator with its obliquity near  $180^\circ$ , so the vertical dashed line in the middle of the plot corresponds to the evening terminator. Benu is assumed to be shaped like a sphere. The direction of the Sun and local noon are defined by 12 pm, whereas the anti-Sun direction is 12 am (midnight). Ecliptic north and south are at the top and bottom of the plot. Most impacts should occur in the late afternoon near the terminator.

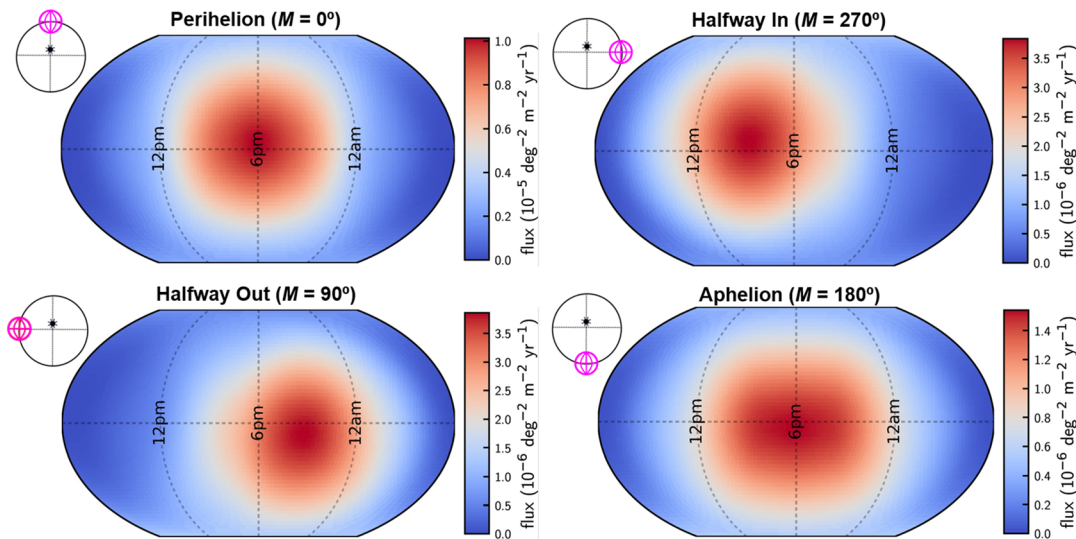


**Figure 8.** The directionality of the meteoroid impact flux across the surface of Benu at different locations on its orbit for a limiting kinetic energy of 7 kJ. The coordinate system is the same as described in Figure 7. The location of Benu in its orbit is described by the label on each figure, the mean anomaly  $M$ , and the small inset of Benu orbit, where Benu is the purple circle. The scale bar decreases by an order of magnitude between perihelion, where it is highest, and the other three plots (see also Figure 5). MEM predicts that most impacts occur near perihelion, impacts on the outbound orbit skew to the evening, while impacts on the inbound orbit skew to the early afternoon.

found that the fast impacts tend to produce small, deep craters without spallation. Shock-induced melting can also occur, which can lead to a decrease in the reflectance of the material (e.g., see also Pieters & Noble, 2016).

Other Van de Graaff accelerator experiments show that tiny impacts can produce plasma. For example, Fletcher et al. (2015) find that for speeds larger than  $18 \text{ km s}^{-1}$ , target material behind the shock front produced by the hypervelocity impact can be vaporized and ionized. The volume of plasma produced in a micron-sized impact event is a function of impact velocity. When energy densities are high, the production of ejecta can be suppressed, with considerable energy going into plasma production. These results also explain why some have used laboratory laser ablation experiments as a proxy for micron-sized impact events to study space weathering; the energy and energy densities are comparable (e.g., Moroz et al., 1996; additional references can be found in Pieters & Noble, 2016). In laser experiments, plasma production is common, and ejecta production can be minimal (e.g., Fletcher et al., 2015; Lee et al., 2013). If the experiments above readily scale up to larger impact events, it might be argued that the Holsapple and Housen crater scaling laws should not be used at Benu.

The applicability of the above experiments to millimeter-sized impactors hitting Benu at tens of kilometers per second, however, may be limited. First, for impacts, the strength of the target is far more important at small sizes than at large sizes. Strength generally scales as the inverse square root of the size, and small volumes are inherently stronger than large ones because they are statistically less likely to contain a flaw (e.g., Melosh, 1989). Target strength may inhibit ejecta production for fast-moving micron-sized impacts because the energy produced cannot break out of the target. As we will discuss below, numerical experiments indicate that this is not the case for millimeter-sized impactors.

Second, even when pressures are high enough that some part of the cratered material is converted to vapor or plasma, it does not exclude the production of solid ejecta for larger projectiles. Consider that even if a source region is ionized, the ionized material produces high pressure and blow-out. If the source region is larger than a few times the local size scale, the pressure should be transmitted to the adjacent material, producing ejecta. Also, the physics of micron-sized projectile impacts is dominated by viscosity and may not be similar to that of millimeter-sized projectile impacts (J. Melosh, personal communication; see also Melosh, 1989).

If a millimeter-size particle were to strike a solid rock at a few tens of kilometers per second, one would expect to at least see solid material ejected as spalls around the crater (K. Housen, personal communication).



Depending on the size scale, those spalls could be mineral grains or larger fragments. If the impact occurred in a granular collection of regolith particles (even up to several millimeters in size), some material would be melted, vaporized, or ionized, but there would still be an outgoing shock that would set material in motion, causing ejection of solid grains away from the impact site.

Third, although laser ablation is often claimed to simulate impacts, a detailed comparison does not support this contention, particularly for larger impactors (J. Melosh, K. Housen, K. Holsapple, personal communication). Lasers can produce the specific energies of high-speed impacts. Laser deposition is a function of pulse duration. Femtosecond pulses deposit energy in the near surface and so cannot replicate the geometry of the material flow field produced by an impact. With nanosecond pulses, there is enough time for the thermal wave to propagate into the target material and create a molten layer. The resulting vaporization creates a recoil pressure that expels the resulting liquid material (Chichkov et al., 1996). Thus, it is possible to find nanosecond-pulsed laser ablation experiments that produce both plasma and considerable ejecta (e.g., Marston & Pacheco-Vázquez, 2019). This phenomenon is similar to impacts that produce energy deposition at some depth below the surface, which in turn encourages material ejection.

Fourth, consider that a common way to examine what happens in high-velocity impacts is through numerical hydrocode experiments and crater scaling laws. These methods have been tested against laboratory impact experiments, where tested velocities are generally  $<5 \text{ km s}^{-1}$ , and nuclear explosions. The energy densities of the former are an order of magnitude lower than those of the high-speed millimeter-sized impacts discussed here, but the latter are many orders of magnitude higher (i.e., one would have to go to  $\sim 1,000 \text{ km s}^{-1}$  for an impact to equal the energy density of a nuclear bomb). This tells us that numerical hydrocodes and crater scaling laws can handle high-speed impacts.

Numerical impact experiments with the code iSALE (Collins et al., 2004; Wünnemann et al., 2006), where millimeter-sized impactors hit a surface at  $40 \text{ km s}^{-1}$ , show that such impacts produce substantial ejecta (J. Melosh, personal communication). The shock wave, while very strong near the impact point, weakens as it spreads out and generates ejecta just like a slower impact. If energy density were indeed an ejecta inhibitor, we would expect nuclear explosions to produce little ejecta, contrary to observations (Melosh, 1989).

Fifth, millimeter-sized impactors are not small compared to the grain sizes in rocks. In soils, laboratory cratering experiments often use impactors in that size range.

To summarize, our suggested millimeter-sized impacts on Bennu can be considered similar to standard cratering events from laboratory shot experiments, except that their energy density is larger by an approximate factor of 10. Such events, however, are well within the tolerance range of existing crater scaling laws.

### 5.1.2. Impact Results Using the Holsapple and Housen Web Application

Our input into the Impact and Explosion Effects web application is as follows. The diameters of the projectiles were assumed to be 2.6 and 1.6 mm for bulk densities of  $860 \text{ kg m}^{-3}$  and  $3,800 \text{ kg m}^{-3}$ , respectively. The typical impact velocity was set to  $43 \text{ km s}^{-1}$ . Bennu's diameter and bulk density were chosen to be 490 m and  $1,190 \text{ kg m}^{-3}$ , respectively (Lauretta, DellaGiustina, et al., 2019). These values reproduce Bennu's mass of  $7.33 \times 10^{10} \text{ kg}$ . We tested the impactors described at the beginning of the section with impact angles that were vertical (defined as  $0^\circ$  in the coordinate system of the web tool) and  $45^\circ$  to the surface.

When we assumed that Bennu's surface material acts like generic soil, which the model assigns as having cohesion of  $10,000 \text{ dynes cm}^{-2}$ , a friction angle of  $33^\circ$ , and a porosity of 30%, our impactors created a crater 14 to 16.1 cm in diameter. This crater size cannot yet be resolved from surface images but may be better explored when high-resolution images of the sample site are returned. The volume of the crater was 260 to  $390 \text{ cm}^3$ , the time of formation was 22 to 24 s, and the ejected mass was 230 to 350 g. Only  $\sim 20\%$  of the ejecta launched off of Bennu reached velocities  $>3.3 \text{ m s}^{-1}$ , the upper limit of the observed particle velocities. This suggests that the observed particles may represent most of the ejected mass.

Placing all of the ejecta into a single object yielded a body 8 to 9.2 cm in diameter, a reasonable match to the approximate sizes of the largest particles observed in orbit around Bennu (i.e., recent calculations suggest the largest particle was about 6 cm, with a small number of particles between 2 and 4 cm; S. Chesley, personal communications). This size can also be considered a good match to all of the ejected material if (i) the ejecta size distribution followed a power law with a shallow slope, which seems to be a reasonable approximation

for the observed particles (Lauretta, Hergenrother, et al., 2019), and (ii) and very little material escaped Bennu prior to OSIRIS-REx observations.

When instead we assumed that the impactor hit generic rock, which the code assigns a cohesion of  $1 \times 10^9$  dynes  $\text{cm}^{-2}$ , a friction angle of  $40^\circ$ , and a porosity of 0%, it created a so-called spall crater  $\sim 6$  to  $7$  cm in diameter. The volume of the crater was much smaller, with a range of  $2$  to  $3.6 \text{ cm}^3$  for the different projectile types. Nearly all of the mass was ejected at velocities  $> 3.3 \text{ m s}^{-1}$ , leaving few sizable particles on orbits that could be seen by OSIRIS-REx.

Our takeaway is that impacts onto Bennu materials can potentially reproduce the largest observed particle ejection events if the majority of rocks and materials getting hit are highly porous and structurally weak. This seems likely based on different lines of evidence.

First, we consider Hayabusa2's Small Carry-on Impactor experiment on Ryugu, where a 2.5-kg copper plate was shot into Ryugu at  $2 \text{ km s}^{-1}$ . It made a crater that was 13–17 m in diameter, with the latter value a rim to rim measurement (Arakawa et al., 2020). If we convert the plate mass into a comparable comet projectile (i.e., 0.17 m for  $800 \text{ g cm}^{-3}$ ), it yields a crater to projectile ratio of  $\sim 76$ – $100$ . This value is so large that the Hayabusa2 team suggested Ryugu's surface acts like it has the same strength as cohesionless sand upon impact. In comparison, in our web tool calculations above, our 1.6- to 2.6-mm projectiles made a 14- to 16.1-cm crater, yielding nearly the same crater to projectile ratio as the Small Carry-on Impactor experiment (i.e., 53–100). The similarity of these results suggests our chosen surface properties for Bennu are reasonable.

Second, laboratory impact experiments, where high-velocity projectiles were fired into hydrated porous meteorites, tend to produce far more dust and debris than nonhydrated nonporous targets (Tomeoka et al., 2003). This fits with observations of boulders on Ryugu, where some boulders have estimated porosities as large as 55% (Grott et al., 2019). If such high porosity values are eventually confirmed by sample analysis, new crater scaling laws may be needed to accommodate the nature of meteoroid impacts on Bennu.

## 5.2. Meteoroid Impacts on Other Airless Worlds

Meteoroid impacts on Bennu are consistent with two key constraints that any particle ejection event mechanism must satisfy to explain observations: (i) They produce more energy than observed in the ejected particles, and (ii) they tend to occur in the late afternoon (local time). These conditions are necessary but are not yet sufficient to prove that our scenario is correct. One way to strengthen our arguments is to show that sporadic meteoroid impacts affect additional worlds in ways consistent with our model's predictions.

We start with the Moon. The Lunar Dust Experiment (LDEX) on the NASA Lunar Atmosphere and Dust Environment Explorer (LADEE) observed a secondary dust ejecta cloud orbiting the Moon (Horanyi et al., 2015). It is thought to be created by meteoroid impacts that launch material off the surface of the Moon at high velocities. Most impacts on LDEX were in the micron-size range; LDEX is considered sensitive to particle  $> 0.6 \mu\text{m}$  in diameter. Szalay and Horanyi (2015) estimate that the ratio between the total mass of ejected material reaching LDEX to the mass of the impacting particle is 1,000 for vertical impacts.

The lunar debris cloud has an asymmetric shape (e.g., Janches et al., 2018). It was found to be most dense at 5 to 8 hr of lunar local time, 4 to 7 hr before lunar noon. This time range is essentially a reverse image of what was observed on Bennu, where the largest particle ejection events occurred 3.5 to 6 hr after local noon. The difference is that the Moon spins in a prograde sense, with an obliquity with respect to its orbital plane of  $6.68^\circ$ , whereas Bennu revolves in a retrograde sense, with an obliquity of  $177.6^\circ$ . Cometary particles should produce head-on collisions with both worlds, with the spin axis modifying the particle ejection times accordingly.

Numerical modeling work using LADEE data indicates that sporadic meteoroids from the helion, antihelion, and apex sources are the source of the lunar ejecta cloud (Janches et al., 2018; Szalay & Horanyi, 2015). In a recent modeling effort, Janches et al. (2018) showed that a 1.3:1 ratio of short-period comet to long-period comet particles striking the Moon was sufficient to reproduce the shape of the near-dawn-centered peak in the ejecta cloud recorded by LDEX observations. Given that meteoroid impacts are capable of launching small lunar particles to orbits where LDEX can detect them, it is reasonable to assert that the same mechanism can work on Bennu.

A similar effect is seen on Mercury, where impacts from cometary particles have been proposed to be a potential source of Mercury's exosphere (Pokorný et al., 2017, 2018). Pokorný et al. (2018) used numerical models to track the evolution of particles coming from Jupiter-family comets, nearly isotropic comets, and main belt asteroids. When particles strike Mercury at high velocities, they vaporize themselves and some target material. The model predicts that there should be a strong preference for vaporization centered near 6 am (6 hr before local noon), much like that seen on the Moon. The model results are consistent with the large dawn/dusk asymmetry in Mercury's exosphere observed by MESSENGER (Burger et al., 2014; Merkel et al., 2017).

Pokorný et al. (2018) also find the impact vaporization pattern on Mercury should vary as Mercury evolves along its eccentric orbit ( $e = 0.205$ , almost the same as Benu). At perihelion and aphelion, impacts are centered at the dawn terminator (6 am, or 6 hr before local noon). When Mercury is moving outward away from the Sun and toward aphelion, the impacts shift to the early morning, with a maximum displacement occurring at 3 am (9 hr before local noon). When it is moving toward perihelion, the impacts move back to the dayside, with maximum displacement at 9 am (3 hr before local noon).

Much like the lunar LDEX data, these results can be considered a reverse image of the MEM results for Benu. Like the Moon, Mercury has a prograde spin, as opposed to Benu's retrograde spin. In particular, the Pokorný et al. (2018) description of how the vaporization pattern for Mercury should change along its eccentric orbit are consistent with our Figure 5 results, with Benu an opposite or "doppelgänger" of Mercury's pattern.

Concerning asteroids, particle ejection events have only been detected on Benu thus far, though this is likely an observational selection effect. OSIRIS-REx looked for satellites during its approach to Benu, but its instruments did not have the sensitivity to detect most of the particles found at closer distances. When OSIRIS-REx entered into Benu's orbit and began observations, the spacecraft was approximately 1.5 km away from Benu. The particles were seen in long-exposure images (5 s) used to observe background star fields for spacecraft navigation in orbit. The Near Earth Asteroid Rendezvous mission, Hayabusa, and Hayabusa2 missions to Eros, Itokawa, and Ryugu, respectively, did not attempt comparable search strategies at such distances and so were unlikely to be able to detect <10 cm particles in orbit. It was also fortuitous that the initial search by OSIRIS-REx near Benu occurred near Benu's perihelion, as MEM results predict that Benu experiences the highest impact rate at that orbital location (Figures 5 and 8).

With that said, Szalay and Horanyi (2016)—using a numerical model once used to simulate the origin of particles detected with the LDEX results on LADEE—predicted that most asteroids should be surrounded by a small steady-state dust cloud of submicron-sized particles concentrated in the body's apex direction. The number density from this putative cloud may be high enough that a spacecraft with a sensitive dust detector might be able to hit a few during a close flyby.

### 5.3. Meteoroid Impact Effects on Benu

Our MEM results support the idea that Benu is frequently struck by sporadic meteoroids traveling at very high velocities. The same should be true for other near-Earth objects, such as those visited by spacecraft missions (e.g., Ryugu), and main belt asteroids. This possibility raises questions about what our expectations should be for samples returned from Benu and Ryugu.

To this end, it is useful to first consider the nature of lunar regolith samples returned by the Apollo astronauts. Once new rocks emerge on the lunar surface from a lava flow, they are immediately battered by high-velocity meteoroids. These impacts break the rocks down into a fragmental layer of material. The high collision velocities also melt and alter some of the target surface debris. Eventually, this creates a thin regolith. As time goes on, only the most energetic impacting particles can access the coherent rock below. This means regolith depth will only slowly increase while steadily mixing surface debris together.

Meteoroid impacts onto the Moon also produce agglutinates, defined as lunar particles bonded together by regolith melt that takes the form of vesicular, flow-banded glass (McKay et al., 1991). The vesicles come from the release of solar wind-implanted gases. Agglutinates tend to be tens of microns to a few millimeters in diameter and resemble the lunar soil's bulk composition. On average, they make up 25% to 30% of the volume of lithic fragments in lunar regolith samples but can range from 0% at fresh craters to 60% for mature soils

(Lucey, 2006). Agglutinates also produce spectral darkening with little or no wavelength dependence (Pieters & Noble, 2016).

Although some meteorites from asteroids show evidence that they were derived from regolith-like deposits, chondrites show limited evidence for agglutinate-type soil melts or components that would correspond to grain-boundary melts and their accompanying fine-grained opaques (McKay et al., 1989, 1991). It has been argued that the reason for this is related to impact velocities, which are lower in the main belt than on the Moon for asteroid impacts ( $\sim 5 \text{ km s}^{-1}$  vs.  $\sim 20 \text{ km s}^{-1}$  on the Moon; Bottke et al., 1994, 2002). Asteroids produce little melt at  $5 \text{ km s}^{-1}$  (Marchi et al., 2013), and as such agglutinates should be rare (e.g., Horz et al., 2005). The problem with this argument is that the sporadic meteoroids are bombarding main belt asteroids, near-Earth asteroids, and the Moon at roughly comparable velocities. If meteoroids make agglutinates in the lunar regolith, one might expect to see similar kinds of particles on asteroids.

The absence of agglutinates in asteroid meteorites might be explained by applying what we have learned about small asteroids and the meteorite delivery process.

First, current models indicate that most meteorite precursors come from asteroid families in the main belt via a collisional cascade (Bottke et al., 2015). When a parent body disrupts in the main belt, it creates numerous smaller fragments that then begin to drift by the Yarkovsky effect toward resonances that can take them to Earth. The net surface area of these families represents a larger surface area than the parent body itself, so one might argue that family members make a better platform for forming agglutinates than the parent body. Observations of the surfaces of Bennu, Ryugu, and Itokawa, however, indicate that they do not have a lunar-like regolith but instead are generally deficient in the very small particles that need to be fused together to make agglutinates (e.g., Lauretta, DellaGiustina, et al., 2019). Any material broken up on the Moon will likely stay bound to the surface, whereas on small asteroids, this material will likely escape via interactions with the solar wind and electrostatic levitation (e.g., Schwan et al., 2017; Wang et al., 2016). Accordingly, although the immediate precursors of meteorites may be dominated by surface rocks and boulders, their paucity of small regolith-like surface particles may prevent them from forming agglutinates.

A second nonexclusive possibility may be “Bogard’s rule,” as defined by Scott and Bottke (2011). Using the meteorite record as a guide, Don Bogard argued that smaller bodies undergo fewer large impacts and lose ejecta more readily than bigger bodies. They also undergo limited impact heating from high-velocity projectiles (Marchi et al., 2013). Bogard’s rule implies that small bodies are much less likely to produce fragmental breccias via impact (shock) heating on the surface of the body. Instead, the fragmental breccias that do exist may have formed during asteroid disruption and reassembly events where surface material may be a small fraction of the entire volume of the body undergoing impact heating (McKay et al., 1989).

Bogard’s rule explains why the breccia fraction increases from Angrites (possibly from a parent body that was destroyed early in solar system history, leaving behind smaller bodies), to H chondrites (possibly from an intact  $>200\text{-km}$ -diameter body in the main belt today), to eucrites (likely from the  $530\text{-km}$ -diameter asteroid Vesta), to lunar samples (an intact world that is  $3,476 \text{ km}$  in diameter). Most of the accessible lunar rocks on the Moon are breccias formed by impact events (McKay et al., 1989). Accordingly, even if agglutinates could form on the surface of a small asteroid, they would rarely fuse together to form a strong meteorite precursor that could reach Earth.

Taking these lines of reasoning together, we predict the byproducts of meteoroid impacts seen within samples from Bennu or Ryugu will take the form of microcraters, pits, and/or physical or chemical changes to the surface of a rock where the impactor hit. We argue that agglutinate-like particles should also be rare but perhaps not completely absent given the high velocities of sporadic meteoroid impacts. An examination of Bennu and Ryugu samples for high-velocity impact heating or melting byproducts would be revealing.

#### 5.4. Volatile-Rich Asteroid Disruption Near the Sun Assisted by Meteoroid Impacts?

In a new model of the near-Earth object population, Granvik et al. (2016) demonstrated that many subkilometer low-albedo near-Earth objects catastrophically disrupt when they reach perihelion  $q < 0.05$  to  $0.2 \text{ au}$ . The precise destruction mechanism is a mystery, but there could be connections to the volatile-rich nature of low-albedo asteroids and the high temperatures that they reach close to the Sun (i.e., for perihelion  $q < 0.2 \text{ au}$ , surface temperatures can exceed  $900 \text{ K}$ ; Figure 4; Delbo & Michel, 2011). Ye and Granvik (2019) also argued that the disruption of such objects explains the overabundance of

Sun-approaching meteor showers, provided they undergo an extended disintegration phase that lasts up to a few thousand years.

Insights into the behavior of primitive asteroids at high temperatures can be gleaned from laboratory heating experiments on volatile-rich carbonaceous chondrites. For example, Garenne et al. (2014) performed thermogravimetric analysis on 26 CM chondrites, 7 CR chondrites, and 1 CI; these meteorites cover a wide range of aqueous alteration (scale of 2.0 to 2.6; Rubin et al., 2007). They were crushed and heated, with volatile loss and sample behavior measured as temperatures were increased. Overall, Garenne et al. (2014) found substantial net mass losses from CM and CR meteorites (~12 to 17 wt.%), with considerable mass release of hydroxyl groups bound in phyllosilicates at temperature  $T = 400^{\circ}\text{C}$  to  $770^{\circ}\text{C}$  and the release of  $\text{CO}_2$  in calcium carbonates at  $T = 770^{\circ}\text{C}$  to  $900^{\circ}\text{C}$ .

Extreme volatile loss should damage the structural integrity of surface boulders, with desiccated boulders possibly more likely to fall apart or shed surface mass from thermal cracking (e.g., Delbo et al., 2014). Some may even eject material away from the asteroid at escape velocity (e.g., Lauretta, Hergenrother, et al., 2019). However, thermal models suggest that seasonal heat waves may only penetrate to depths of some tens of centimeters to perhaps a few meters for some bodies (e.g., Nesvorný & Bottke, 2004; Vokrouhlický, 1998); silicates below the surface layer may remain solid. To achieve further disruption, additional processes may be needed to break down the boulder and steadily remove surface material, thereby preventing the development of an inert volatile-free surface lag.

We postulate that meteoroid impacts may be effective in breaking down rocks and debris weakened by thermal cracking. Material taking the form of submillimeter particles can subsequently be ejected from the body over relatively short time scales by electrostatic levitation (i.e., the interaction of solar wind plasma and UV radiation with the asteroids' surfaces and their near-zero surficial gravity; Hartzell & Scheeres, 2013; Hartzell, 2019). The latter effect likely explains why Bennu and Ryugu lack fine-grained materials on their surfaces (Grott et al., 2019; Lauretta, DellaGiustina, et al., 2019).

All these mechanisms, working in concert, may help explain why low-albedo asteroids are eliminated close to the Sun. It might also explain why higher-albedo asteroids that are volatile poor (i.e., bodies composed of ordinary chondrite material) are apparently better at surviving close to the Sun (e.g., Granvik et al., 2016). Their boulders and rocks remain strong, relatively speaking, and meteoroid impacts produce less cumulative damage.

Impacts may also have the ability to crack the surface of a rock and/or create a "bullet hole" in a boulder that would allow interior volatiles to more readily escape. If true, rocks damaged by meteoroid impacts should have different physical and volatile properties than those that have avoided such collisions. The samples returned by the OSIRIS-REx and Hayabusa2 missions may enable insights into this issue.

## 6. Conclusions

Here we briefly recap our main conclusions:

1. Meteoroids derived from cometary sources are capable of striking Bennu near perihelion once every 2 weeks on average with an average impact  $KE$  of 7,000 J. That energy is comparable to a 12-gauge shotgun blast.
2. The majority of these impactors strike Bennu in the late afternoon near its perihelion. This matches the timing of the three largest particle ejection events observed on Bennu to date (between December 2018 and February 2019), which occurred 3.5 to 6 hr after local noon (Lauretta, Hergenrother, et al., 2019).
3. If Bennu's surface material acts like generic soil in impacts, cometary meteoroids can eject sufficient mass to explain the sizes of the largest observed particles found on temporary orbits around Bennu in the largest observed particle ejection events (<10 cm). This may suggest that many rocks and boulders on Bennu are structurally weak and highly porous.
4. We predict that fewer large particle ejection events will occur as Bennu moves toward aphelion and that the timing of the events will skew toward the evening and morning on the outbound and inbound side of its orbit, respectively.
5. Our result suggest that high-energy meteoroids should strike all near-Earth objects at high velocities. We postulate that samples returned from Bennu and Ryugu by the OSIRIS-REx and Hayabusa2 missions

may show evidence for these collision events in the form of microcraters, pits, fractures, melt products, and/or physical or chemical changes to the rock where the impactor hit. Our expectation is also that boulders on the surfaces of these bodies should show comparable effects produced by high-velocity impactors.

- The absence of obvious evidence for lunar-like agglutinates thus far on near-Earth objects may suggest that these worlds do not have numerous fine particles located on their surfaces (i.e., they lack a lunar-like regolith).

#### Acknowledgments

We thank Keith Holsapple, Kevin Housen, and Jay Melosh for their comments that helped us to better understand the nature of hypervelocity impacts for micron- and millimeter-sized bodies. We also thank Peter Brown and an anonymous referee for their helpful and constructive comments. We are grateful to the OSIRIS-REX Team for making the encounter with Bennu possible. The Meteoroid Engineering Model is publicly available from NASA's Meteoroid Environment Office upon request ([https://www.nasa.gov/offices/meo/software/mem\\_detail.html](https://www.nasa.gov/offices/meo/software/mem_detail.html)). The data generated in this work are reported in the text and figures. Model data and other numerical values can be found at the figshare repository: <https://doi.org/10.6084/m9.figshare.11819448> (see Bottke, 2020). This paper is based upon work supported by NASA's OSIRIS-REX mission through NASA Contract NNM10AA11C issued through the New Frontiers Program and Grant No. 80NSSC18K0226 as part of the OSIRIS-REX Participating Scientist Program. The work of David Vokrouhlický was partially funded by Grant 18-06083S of the Czech Science Foundation.

#### References

- Arakawa, M., Saiki, T., Wada, K., Ogawa, K., Kadono, T., Shirai, K., et al. (2020). An artificial impact on the asteroid (162173) Ryugu formed a crater in the gravity-dominated regime. *Science*, *368*(6486), 67–71. <https://doi.org/10.1126/science.aaz1701>
- Barnouin, O. S., Daly, M. G., Palmer, E. E., Gaskell, R. W., Weirich, J. R., Johnson, C. L., et al. (2019). Shape of (101955) Bennu indicative of a rubble pile with internal stiffness. *Nature Geoscience*, *12*(4), 247–252. <https://doi.org/10.1038/s41561-019-0330-x>
- Bottke, W. F. (2020). *Run results for NASA's meteoroid engineering model where meteoroids are striking the asteroid Bennu*. <https://doi.org/10.6084/m9.figshare.11819448>
- Bottke, W. F., Brož, M., O'Brien, D. P., Campo Bagatin, A., Morbidelli, A., & Marchi, S. (2015). The collisional evolution of the asteroid belt. In P. Michel, F. DeMeo, & W. F. Bottke (Eds.), *Asteroids IV* (pp. 701–724). Tucson: U. Arizona Press. [https://doi.org/10.2458/azu\\_uapress\\_9780816532131-ch036](https://doi.org/10.2458/azu_uapress_9780816532131-ch036)
- Bottke, W. F., Morbidelli, A., Jedicke, R., Petit, J.-M., Levison, H., Michel, P., & Metcalfe, T. S. (2002). Debaised orbital and size distributions of the near-Earth objects. *Icarus*, *156*, 399–433.
- Bottke, W. F., Nolan, M. C., Kolvoord, R. A., & Greenberg, R. (1994). Velocity distribution among colliding asteroids. *Icarus*, *107*, 255–268.
- Burger, M. H., Killen, R. M., McClintock, W. E., Merkel, A. W., Vervack, R. J., Cassidy, T. A., & Sarantos, M. (2014). Seasonal variations in Mercury's dayside calcium exosphere. *Icarus*, *238*, 51–58.
- Campbell-Brown, M. D. (2008). High resolution radiant distribution and orbits of sporadic radar meteoroids. *Icarus*, *196*, 144–163.
- Chichkov, B. N., Momma, C., Nolte, S., Alvensleben, F., & Tünnermann, A. (1996). Femtosecond, picosecond and nanosecond laser ablation of solids. *Applied Physics A*, *63*(2), 109–115. <https://doi.org/10.1007/BF01567637>
- Collins, G. S., Melosh, H. J., & Ivanov, B. A. (2004). Modeling damage and deformation in impact simulations. *Meteoritics & Planetary Science*, *39*, 217–231.
- Delbo, M., Libourel, G., Wilkerson, J., Murdoch, N., Michel, P., Ramesh, K. T., et al. (2014). Thermal fatigue as the origin of regolith on small asteroids. *Nature*, *508*(7495), 233–236. <https://doi.org/10.1038/nature13153>
- Delbo, M., & Michel, P. (2011). Temperature history and dynamical evolution of (101955) 1999 RQ36: A potential target for sample return from a primitive asteroid. *The Astrophysical Journal*, *728*, L42.
- Fiege, K., Guglielmino, M., Altobelli, N., Trieloff, M., Srama, R., & Orlando, T. M. (2019). Space weathering induced via microparticle impacts: 2. Dust impact simulation and meteorite target analysis. *Journal of Geophysical Research: Planets*, *124*, 1084–1099.
- Fletcher, A., Close, S., & Mathias, D. (2015). Simulating plasma production from hypervelocity impacts. *Physics of Plasmas*, *22*, 093504.
- Garenne, A., Beck, P., Montes-Hernandez, G., Chiriach, R., Toche, F., Quirico, E., et al. (2014). The abundance and stability of water in type 1 and 2 carbonaceous chondrites (CI, CM and CR). *Geochimica et Cosmochimica Acta*, *137*, 93–112. <https://doi.org/10.1016/j.gca.2014.03.034>
- Granvik, M., Morbidelli, A., Jedicke, R., Bolin, B., Bottke, W. F., Beshore, E., et al. (2016). Super-catastrophic disruption of asteroids at small perihelion distances. *Nature*, *530*(7590), 303–306. <https://doi.org/10.1038/nature16934>
- Grott, M., Knollenberg, J., Hamm, M., Ogawa, K., Jaumann, R., Otto, K. A., et al. (2019). Low thermal conductivity boulder with high porosity identified on C-type asteroid (162173) Ryugu. *Nature Astronomy*, *3*(11), 971–976. <https://doi.org/10.1038/s41550-019-0832-x>
- Grün, E., Zook, H. A., Fechtig, H., & Giese, R. H. (1985). Collisional balance of the meteoritic complex. *Icarus*, *62*, 244–272.
- Hamilton, V. E., Simon, A. A., Christensen, P. R., Reuter, D. C., Clark, B. E., Barucci, M. A., et al. (2019). Evidence for widespread hydrated minerals on asteroid (101955) Bennu. *Nature Astronomy*, *3*(4), 332–340. <https://doi.org/10.1038/s41550-019-0722-2>
- Hartzell, C. M. (2019). Dynamics of 2D electrostatic dust levitation at asteroids. *Icarus*, *333*, 234.
- Hartzell, C. M., & Scheeres, D. J. (2013). Dynamics of levitating dust particles near asteroids and the Moon. *Journal of Geophysical Research: Planets*, *118*, 116–125. <https://doi.org/10.1029/2012JE004162>
- Holsapple, K. A. (1980). *The equivalent depth of burst for impact cratering* (pp. 2379–2401). Paper presented at Lunar and Planetary Science Conference, 11th, Houston, TX.
- Holsapple, K. A. (1993). The scaling of impact processes in planetary sciences. *Annual Review of Earth and Planetary Sciences*, *21*, 333–373.
- Holsapple, K. A., & Housen, K. R. (2013). *The third regime of cratering: Spall craters* (p. 2733). Paper presented at 44th Lunar and Planetary Science Conference, The Woodlands, TX.
- Holsapple, K. A., & Schmidt, R. M. (1980). On the scaling of crater dimensions. 1. Explosive processes. *Journal of Geophysical Research*, *85*, 7247–7256.
- Holsapple, K. A., & Schmidt, R. M. (1982). On the scaling of crater dimensions. 2. Impact processes. *Journal of Geophysical Research*, *87*, 1849–1870.
- Horányi, M., Szalay, J. R., Kempf, S., Schmidt, J., Grün, E., Srama, R., & Sternovsky, Z. (2015). A permanent, asymmetric dust cloud around the Moon. *Nature*, *522*(7556), 324–326. <https://doi.org/10.1038/nature14479>
- Horz, F., Cintala, M. J., See, T. H., & Le, L. (2005). Shock melting of ordinary chondrite powders and implications for asteroidal regoliths. *Meteoritics and Planetary Science*, *40*, 1329–1346.
- Housen, K. R., & Holsapple, K. A. (1999). Scale effects in strength-dominated collisions of rocky asteroids. *Icarus*, *142*, 21–33.
- Housen, K. R., & Holsapple, K. A. (2011). Ejecta from impact craters. *Icarus*, *211*, 856–875. <https://doi.org/10.1016/j.icarus.2010.09.017>
- Housen, K. R., Schmidt, R. M., & Holsapple, K. A. (1983). Crater ejecta scaling laws—Fundamental forms based on dimensional analysis. *Journal of Geophysical Research*, *88*, 2485–2499.

- Janches, D., Pokorný, P., Sarantos, M., Szalay, J. R., Horanyi, M., & Nesvorný, D. (2018). Constraining the ratio of micrometeoroids from short- and long-period comets at 1 AU from LADEE observations of the lunar dust cloud. *Geophysical Research Letters*, *45*, 1713–1722. <https://doi.org/10.1002/2017GL076065>
- Jenniskens, P., Nénon, Q., Albers, J., Gural, P. S., Haberman, B., Holman, D., et al. (2016). The established meteor showers as observed by CAMS. *Icarus*, *266*, 331–354. <https://doi.org/10.1016/j.icarus.2015.09.013>
- Jones, J. (2004). *Meteoroid engineering model—Final report (NASA SEE/CR-2004-40048)*. Huntsville, AL: NASA Marshall Space Flight Center.
- Jones, J., Brown, P., Ellis, K. J., Webster, A. R., Campbell-Brown, M., Krzemenski, Z., & Weryk, R. J. (2005). The Canadian Meteor Orbit Radar: System overview and preliminary results. *Planetary and Space Science*, *53*, 413–421.
- Lauretta, D. S., Balram-Knutson, S. S., Beshore, E., Boynton, W. V., Drouet d'Aubigny, C., DellaGiustina, D. N., et al. (2017). OSIRIS-REx: Sample return from asteroid (101955) Bennu. *Space Science Reviews*, *212*(1–2), 925–984. <https://doi.org/10.1007/s11214-017-0405-1>
- Lauretta, D. S., Bartels, A. E., Barucci, M. A., Bierhaus, E. B., Binzel, R. P., Bottke, W. F., et al. (2015). The OSIRIS-REx target asteroid (101955) Bennu: Constraints on its physical, geological, and dynamical nature from astronomical observations. *Meteoritics & Planetary Science*, *50*(4), 834–849. <https://doi.org/10.1111/maps.12353>
- Lauretta, D. S., DellaGiustina, D. N., Bennett, C. A., Golish, D. R., Becker, K. J., Balram-Knutson, S. S., et al. (2019). The unexpected surface of asteroid (101955) Bennu. *Nature*, *568*(7750), 55–60. <https://doi.org/10.1038/s41586-019-1033-6>
- Lauretta, D. S., Hergenrother, C. W., Chesley, S. R., Leonard, J. M., Pelgrift, J. Y., Adam, C. D., et al. (2019). Episodes of particle ejection from the surface of the active asteroid (101955) Bennu. *Science*, *366*(6470), eaay3544. <https://doi.org/10.1126/science.aay3544>
- Lee, N., Close, S., Goel, A., Lauben, D., Linscott, I., Johnson, T., et al. (2013). Theory and experiments characterizing hypervelocity impact plasmas on biased spacecraft materials. *Physics of Plasmas*, *20*, 032901.
- Leinert, C., Richter, I., Pitz, E., & Planck, B. (1981). The zodiacal light from 1.0 to 0.3 A.U. as observed by the HELIOS space probes. *Astronomy and Astrophysics*, *103*, 177–188.
- Lucey, P. (2006). Understanding the lunar surface and space-moon interactions. *Reviews in Mineralogy and Geochemistry*, *60*, 83–219.
- Marchi, S., Bottke, W. F., Cohen, B. A., Wünnemann, K., Kring, D. A., McSween, H. Y., et al. (2013). High-velocity collisions from the lunar cataclysm recorded in asteroidal meteorites. *Nature Geoscience*, *6*(4), 303–307. <https://doi.org/10.1038/ngeo1769>
- Marston, J. O., & Pacheco-Vázquez, F. (2019). Millimetric granular craters from pulsed laser ablation. *Physical Review E*, *99*(3). <https://doi.org/10.1103/physreve.99.030901>
- McKay, D. S., Heiken, G., Basu, A., Blanford, G., Simon, S., Reedy, R., et al. (1991). The lunar regolith. In G. Heiken, D. T. Vaniman, & B. M. French (Eds.), *The lunar sourcebook* (pp. 285–356). New York, NY: Cambridge University Press.
- McKay, D. S., Swindle, T. D., & Greenberg, R. (1989). Asteroidal regoliths—What we do not know. *Asteroids II*, 617–642.
- McNamara, H., Suggs, R., Kauffman, B., Jones, J., Cooke, W., & Smith, S. (2005). Meteoroid Engineering Model (MEM): A meteoroid model for the inner Solar System. *Earth, Moon, and Planets*, *95*, 123–139.
- Melosh, H. J. (1989). *Impact cratering: A geologic process*. New York: Oxford University Press; Oxford: Clarendon Press.
- Merkel, A. W., Cassidy, T. A., Vervack, R. J., McClintock, W. E., Sarantos, M., Burger, M. H., & Killen, R. M. (2017). Seasonal variations of Mercury's magnesium dayside exosphere from MESSENGER observations. *Icarus*, *281*, 46–54.
- Molaro, J. L., Hergenrother, C. W., Chesley, S. R., Walsh, K. J., Hanna, R. D., Haberle, C. W., et al. (2020). Thermal fatigue as a driving mechanism for activity on asteroid Bennu. *Journal of Geophysical Research: Planets*. <https://doi.org/10.1029/2019JE006325>
- Moorhead, A. V., Cooke, W. J., & Campbell-Brown, M. D. (2017). *Meteor shower forecasting for spacecraft operations* (p. 11). Paper presented at 7th European Conference on Space Debris.
- Moorhead, A. V., Kingery, A., & Ehler, S. (2020). NASA's meteoroid engineering model 3 and its ability to replicate spacecraft impact rates. *Journal of Spacecraft and Rockets*, *57*(1), 160–176. <https://doi.org/10.2514/1.a34561>
- Moroz, L. V., Fisenko, A. V., Semjonova, L. F., Pieters, C. M., & Korotaeva, N. N. (1996). Optical effects of regolith processes on S-asteroids as simulated by laser shots on ordinary chondrite and other mafic materials. *Icarus*, *122*, 366–382.
- Nesvorný, D., & Bottke, W. F. (2004). Direct detection of the Yarkovsky effect for main belt asteroids. *Icarus*, *170*, 324–342.
- Nesvorný, D., Jenniskens, P., Levison, H. F., Bottke, W. F., Vokrouhlický, D., & Gounelle, M. (2010). Cometary origin of the zodiacal cloud and carbonaceous micrometeorites. Implications for hot debris disks. *The Astrophysical Journal*, *713*, 816–836.
- Pierazzo, E., Vickery, A. M., & Melosh, H. J. (1997). A reevaluation of impact melt production. *Icarus*, *127*, 408–423. <https://doi.org/10.1006/icar.1997.5713>
- Pieters, C. M., & Noble, S. K. (2016). Space weathering on airless bodies. *Journal of Geophysical Research: Planets*, *121*, 1865–1884. <https://doi.org/10.1002/2016JE005128>
- Pokorný, P., Sarantos, M., & Janches, D. (2017). Reconciling the dawn-dusk asymmetry in Mercury's exosphere with the micrometeoroid impact directionality. *Astrophysical Journal Letters*, *842*, L17.
- Pokorný, P., Sarantos, M., & Janches, D. (2018). A comprehensive model of the meteoroid environment around Mercury. *The Astrophysical Journal*, *863*, 31.
- Rozitis, B., et al. (2020). Implications for ice stability and particle ejection from high-resolution temperature modeling of asteroid (101955) Bennu. *Journal of Geophysical Research: Planets*. <https://doi.org/10.1029/2019JE006323>
- Rubin, A. E., Trigo-Rodríguez, J. M., Huber, H., & Wasson, J. T. (2007). Progressive aqueous alteration of CM carbonaceous chondrites. *Geochimica et Cosmochimica Acta*, *71*, 2361–2382.
- Scheeres, D. J., Britt, D., Carry, B., & Holsapple, K. A. (2015). Asteroid interiors and morphology. In P. Michel, F. DeMeo, & W. F. Bottke (Eds.), *Asteroids IV* (pp. 745–766). Tucson: U. Arizona Press. [https://doi.org/10.2458/azu\\_uapress\\_9780816532131-ch038](https://doi.org/10.2458/azu_uapress_9780816532131-ch038)
- Schmidt, R. M., & Housen, K. R. (1987). Some recent advances in the scaling of impact and explosion cratering. *International Journal of Impact Engineering*, *5*, 543–560.
- Schwan, J., Wang, X., Hsu, H. W., Grün, E., & Horanyi, M. (2017). The charge state of electrostatically transported dust on regolith surfaces. *Geophysical Research Letters*, *44*, 3059–3065. <https://doi.org/10.1002/2017GL072909>
- Scott, E. R. D., & Bottke, W. F. (2011). Impact histories of angrites, eucrites, and their parent bodies. *Meteoritics and Planetary Science*, *46*, 1878–1887.
- Szalay, J. R., & Horanyi, M. (2015). Annual variation and synodic modulation of the sporadic meteoroid flux to the Moon. *Geophysical Research Letters*, *42*, 10,580–10,584. <https://doi.org/10.1002/2015GL066908>
- Szalay, J. R., & Horanyi, M. (2016). The impact ejecta environment of near-Earth asteroids. *The Astrophysical Journal*, *830*, L29.
- Tomeoka, K., Kiriya, K., Nakamura, K., Yamahana, Y., & Sekine, T. (2003). Interplanetary dust from the explosive dispersal of hydrated asteroids by impacts. *Nature*, *423*(6935), 60–62. <https://doi.org/10.1038/nature01567>

- Vokrouhlický, D. (1998). Diurnal Yarkovsky effect as a source of mobility of meter-sized asteroidal fragments. I. Linear theory. *Astronomy & Astrophysics*, 335, 1093–1100.
- Wang, X., Schwan, J., Hsu, H. W., Grün, E., & Horanyi, M. (2016). Dust charging and transport on airless planetary bodies. *Geophysical Research Letters*, 43, 6103–6110. <https://doi.org/10.1002/2016GL069491>
- Wünnemann, K., Collins, G., & Melosh, H. (2006). A strain-based porosity model for use in hydrocode simulations of impacts and implications for transient crater growth in porous targets. *Icarus*, 180, 514–527.
- Ye, Q., & Granvik, M. (2019). Debris of asteroid disruptions close to the Sun. *The Astrophysical Journal*, 873, 104.